Expression and predictive functional profiles on MicroRNAs data in Vascularized Composite Allotransplantation Acute Rejection

Yuan Fang
Central South University
Haibo Li
Central South University
Jingting Chen
Keio University School of Medicine
Yao Xiong
Shanghai Jiao Tong University School of Medicine
Xu Li
Central South University
Binbin Sun
Donghua University
Shengli Li
Shanghai Jiao Tong University School of Medicine
Jianda Zhou
Central South University
Shoubao Wang (wxldragon198418@163.com)
Central South University

Research Article

Keywords: vascularized composite tissue allograft, VCA, miRNAs, acute rejection

Posted Date: May 12th, 2022

DOI: https://doi.org/10.21203/rs.3.rs-1637540/v1

Abstract

Aim: To investigate the mechanisms of acute rejection for vascularized composite allotransplantation (VCA) using microRNAs (miRNAs) differential expression in a VCA animal model.

Methods: Three brown Norway rats were used as transplant donors and three Lewis rats as VCA receptors. The changes were divided into different stages before and after transplantation in Lewis rats. The appearance changes of all subjects were recorded. Also, histological evaluations were performed on all recipients, and the microRNAs expression was analyzed when acute immune rejection occurred. Then, GO and KEGG Pathway analyses were employed to predict miRNA targets. Finally, differentially expressed miRNAs were detected by RT-qPCR.

Results: Compared to pre-operation, 22 miRNAs were screened for significantly different expressions. Among them, nine were upregulated and 13 were downregulated in skin tissues. The RT-qPCR results revealed that rno-miR-340-5p and rno-miR-21-5p were significantly upregulated and enriched in the PI3K-Akt signaling pathway. Moreover, rno-miR-145-5p and rno-miR-195-5p were significantly downregulated, and most of their target genes were enriched in the Hippo signaling pathway. The histological evaluations showed that, after VCA, the skin tissue presented severe acute rejection.

Conclusion: Overall, the miRNAs rno-miR-340-5p, rno-miR-21-5p, rno-miR-145-5p, and rno-miR-195-5p were significantly regulated during VCA acute rejection. These miRNAs are potential biomarkers for objective, early, and minimally invasive rejection diagnosis.

1. Introduction

For some end-stage diseases patients, organ transplantation can be a life-saving choice. In recent decades, the use of immunosuppressive drugs significantly improved the overall survival rate of solid organ transplant recipients [1, 2]. However, compared with other organ transplantation types, vascularized composite allotransplantation (VCA) has a higher incidence of acute rejection [3]. Moreover, few studies regarding why the VCA acute rejection process occurs and how it is regulated are available.

MicroRNAs (miRNAs) are single-stranded noncoding RNAs with 19–25 nucleotides [4]. They are stably present in various tissues and blood. Also, miRNAs can bind to the 3' or 5' untranslated region of a target messenger RNA (mRNA), thereby inhibiting its function or leading to its degradation, finally regulating the occurrence and development of many diseases [5]. Recently, many miRNAs have been related to the activation and regulation of the innate immune system and inflammatory response [6, 7]. Additionally, some reports have shown that the expression of miRNAs in plasma changes during acute rejection after organ transplantation, including heart or kidney [8, 9]. Other studies have reported that plasma miRNA-146a and miRNA-155 can be potential acute rejection biomarkers after VCA [10]. Also, this research team continued to select several differentially expressed miRNAs in plasma for histological diagnosis [11].

However, regarding VCA acute rejection, there is no study with its whole transcriptome sequence and screening differentially expressed miRNAs. Therefore, in the present study, we aimed to evaluate miRNA changes during acute rejection on VCA model rats.

2. Materials And Methods

2.1 Animals

The VCA model was constructed using a rodent hindlimb allograft model. The Shanghai Sippr-BK Laboratory Animal Co. Ltd. (Shanghai, China) provided male Lewis and male Brown Norwegian (BN) rats (200–250 g) for this study. Two different receptors received one hindlimb from the same donor. All animal procedures were approved by the ethics committee of the Ninth People's Hospital Affiliated with the Shanghai Jiao Tong University School of Medicine. This work was performed following the guidelines of the Laboratory Animal Manual of the NIH Guideline for the Care and Use of Laboratory Animals.

2.2 Establishment of the hind limb transplantation model

Before operations, rats were anesthetized by continuous inhalation of isoflurane. Operations were performed as previously described. Briefly, the two hind limbs of donor rats were dissected for the femoral vessels and related nerves, then amputated in the middle of the thigh. Before amputation, the limbs were perfused with cold heparinized Ringer's lactate solution, then stored in the same solution until transplantation. Each hind limb harvested was transplanted *in situ* to isolated recipient rats. The femur was fixed with an 18G intramedullary needle. The dorsal muscle and skin were sutured with a 3 − 0 silk thread. Then the femoral artery, vein, and sciatic nerves were anastomosed with a 12 − 0 nylon thread under an operating microscope. After confirming that the anastomotic vessels were unobstructed, the ventral muscles and skin were sutured with a 3 − 0 silk thread (Fig. 1). Motor and sensory functions were not evaluated in the current study.

Three male BN rats were used as allograft donors and transplantations were performed into three male Lewis rats. The preoperative skin tissue of rats was used as controls. The postoperative skin tissue comprehended the experimental group and was used to analyze the preliminary mechanisms of acute immune rejection.

2.3 Tissue collection and preservation

Pre- and post-operation changes and special conditions observed in mice were daily recorded. After the 7th day, mice were sacrificed. Sterilized scissors were used to collect the skin of experimental mice. Skin tissue pieces were collected from each mouse. Removed skin tissue specimens were divided into two parts and stored. Half of the skin specimen was cut into pieces and frozen in liquid nitrogen for future use. The other half was placed in an EP tube and stored on dry ice for molecular detection. Each skin sample was marked with a corresponding label.

2.4 Hematoxylin and Eosin (H&E) staining

First, fixed skin tissue samples were embedded in paraffin, sectioned (4–5 μm), and mounted on slides. Then, sections were deparaffinized, rehydrated in an ethanol gradient, and stained with H&E trichrome according to standard protocols and using commercially available reagents.

2.5 RNA sequencing (RNA-seq)

The Hiseq Single-End sequencing was used in the present study. First splices were removed and cuts were performed according to the sequence quality. The original sequence was searched using a 5 base length as the window. When the average sequencing base quality in the window was lower than 20, the front end of the window was truncated and discarded. Filtered sequences were further used. Then, the number of clean reads (total reads) with a sequence length of 18–36 nt was counted. Identical sequences in each sample were duplicated and the sequence abundance was assessed. These sequences were called unique reads and were used for subsequent analyses.

2.6 Data collection and analyses

The miRNAs levels were evaluated using sequencing counts and normalized as counts per million of total aligned reads (CPM). Differentially expressed miRNAs were screened based on count values. Hierarchical clustering and Volcano plots were generated using R or Perl environments for statistical computing and graphics.

2.7 Target prediction and functional analyses

MiRNAs can bind to target sites mainly through complementary pairing. To analyze miRNA binding in animals, we predicted the target genes of differentially expressed miRNAs using miRanda and the 3 'UTR' sequence of mRNAs of the species as the target sequence. Top GO was used for GO enrichment analysis. During this analysis, the list of miRNA target genes and the number of miRNA target genes of each term were calculated using differential miRNA target genes annotated by GO term. Then, the *p*-value was calculated by the hypergeometric distribution method (the standard for significant enrichment as *p*-value ≤ 0.05) to find GO terms with significant enrichment of differential miRNA target genes compared to the whole genome background and to determine the main biological functions of these target genes. KEGG pathway enrichment analysis was also performed and the differentially expressed miRNA target genes top 20 pathways with the smallest *p*-values (most significant enriched) were selected.

2.8 Quantitative reverse transcription polymerase chain reaction (RT-qPCR)

First, RNA quality was assessed. Then, total RNA was reverse transcribed into cDNAs (PrimeScript TM 1st stand cDNA Synthesis Kit). Briefly, the reverse transcription reaction system 1 was added to the test tube in ice. Then, 10 μL of RNase-free dH_2O was added. After mixing, samples were incubated at 65°C for 5 min, then quickly placed in an ice bath. Next, the reverse transcription reaction system 2 was added to the test tube in the ice. The reaction was performed at 42°C for 30–60 min. Samples were heated at 95°C for 5 min to end the reaction, then placed into ice for subsequent experiments or cryopreservation. For each target and housekeeping gene, the cDNA template of the sample was selected for PCR reactions (reaction

A). The PCR reaction solution, configured according to the reaction system A, was placed on the real-time PCR instrument to react. For fluorescence signal measurements, the reaction was performed at 95°C for 5 min, then cycled 40 times at 95°C for 15 s and 60°C for 30 s.

2.9 Statistical analyses

Data are presented as means ± standard deviations (SDs). The miRNA expression followed a discrete distribution. Accordingly, significant differences between groups were compared using the negative binomial distribution. Differentially expressed miRNAs were screened based on count values. The significance level was set at $p \leq 0.05$.

3. Results

3.1 Skin visual examinations

The cumulative number of recipients with visual skin changes is shown in Fig. 2. The allogeneic transplantation hind limb led to increasingly worsening edema and swelling within a few days. Erythema and blisters appeared on the 7th day after transplantation. On the 10th day, large erythema and blisters areas appeared, and skin keratolysis was observed. On the 14th day, all transplanted hind limbs gradually became blackened and necrotized upward from the fingertip.

3.2 Histological evaluations

On the 7th day, early epidermis changes, necrosis, keratinization, epidermal thickening, lymphocyte infiltration, and basal cell vacuolation were observed in the upper dermis of post-transplant samples. Therefore, Grade I rejection occurred on the 7th day after transplantation. On the 10th day, the HE staining showed mixed small cell infiltration, increased basal cell vacuolation, and that the epidermis fell off. On the 14th day, the skin edema was severe, and mixed cell infiltration and cell necrosis reached Grade III rejection (Fig. 3 and Table 1). The grading was based on the classification system of Büttemeyer et al. (1996).

Table 1
Classification of acute rejection in the tissue samples.

	Day 3	Day 7	Day 10	Day 14
Grade 0	1			
Grade I	2	2		
Grade II		1	2	
Grade III			1	3

3.3 Differentially expressed miRNAs

The miRNA-seq was used to identify miRNA expression levels in control and experimental groups. Precise sample extraction, detection, and quality control processes were performed to control the sample quality through all steps. Then, the miRNA density distribution was used to investigate the expression pattern of all miRNAs in the sample. Overall, most miRNAs were averaged expressed, and low and high miRNAs expressions accounted for a small part of the total. The miRNA expression characteristics in each sample are shown in Fig. 4A.

We used the R heatmap software package for bidirectional cluster analysis of all miRNAs and samples. Clustering was performed according to the expression level of the same miRNA in different samples and the expression pattern of different miRNAs in the same sample. The Euclidean method was used to calculate the distance, and the hierarchical clustering longest distance method (complete linkage) was used for clustering (Fig. 4B).

According to hierarchical clustering results, differential genes were divided into different expression patterns. They were divided into different clusters (the gene expression trend in the same cluster is similar) to obtain gene clustering results. The clustering of upregulated and downregulated miRNAs is shown in Figs. 4C and 4D, respectively. Moreover, the Volcano plots provided a quick visual identification of the miRNAs displaying large and statistically significant magnitude changes (Figs. 4E). The tRF & tiRNA selection criteria included a higher FC, lower q-value, and higher CMP. After summarizing the original data, 22 differentially expressed miRNAs were screened, nine significantly upregulated and 13 significantly downregulated (Table 2).

Table 2
The candidate miRNA of differentially expression for skin.

ID	BaseMean-pre	BaseMean-post	log2FoldChange	p-value	Regulation
rno-miR-142-5p	607.7350535	20846.13996	5.100193949	4.04073E-06	Up
rno-miR-146a-5p	4257.447789	22377.83468	2.394009703	0.014551208	Up
rno-miR-150-5p	685.9368241	3050.408248	2.152854724	0.013889396	Up
rno-miR-16-5p	2315.252696	12261.92583	2.404944014	0.029899796	Up
rno-miR-21-5p	134232.8018	3857194.518	4.844742739	9.68976E-06	Up
rno-miR-3068-3p	190.345222	851.6295895	2.16160772	0.01817161	Up
rno-miR-340-5p	731.1696561	4309.081037	2.559102126	0.013146273	Up
rno-miR-425-5p	299.5530556	2163.664109	2.852593096	0.010611057	Up
rno-miR-451-5p	808.8197018	8849.762591	3.451748708	0.001476382	Up
rno-let-7b-5p	11966.75571	3135.567548	-1.932233575	0.034061084	Down
rno-miR-100-5p	22339.55589	3253.964067	-2.779330281	0.001942897	Down
rno-miR-125a-5p	2917.416179	620.9017359	-2.232254336	0.017164991	Down
rno-miR-125b-2-3p	992.4256572	221.1078847	-2.166208561	0.02065144	Down
rno-miR-125b-5p	6963.711548	1541.142527	-2.175856154	0.017261722	Down
rno-miR-127-3p	10921.39714	530.8676479	-4.362661393	0.000227024	Down
rno-miR-145-3p	770.6204841	156.1568219	-2.303024939	0.012479141	Down
rno-miR-145-5p	1823.94205	225.9399707	-3.013048469	0.001068252	Down
rno-miR-152-3p	31358.13349	9363.154506	-1.74377312	0.042792695	Down
rno-miR-195-5p	1330.00309	204.4803286	-2.701395632	0.003009653	Down
rno-miR-196a-5p	1150.462541	218.8798351	-2.394003057	0.008217532	Down
rno-miR-196b-5p	1149.408863	280.4985988	-2.03482661	0.020797481	Down
rno-miR-379-5p	6844.839945	723.2646587	-3.242421244	0.000549802	Down

3.4 Bioinformatic analyses

Moreover, miRNAs can bind to target sites mainly through complementary pairing. To analyze miRNAs bindings in rats, we used miRanda to target the 3 'UTR' sequence of their mRNAs. Target genes were predicted for differentially expressed miRNA sequences.

The GO enrichment analysis was performed using Top GO. During analysis, the list of miRNA target genes and the number of miRNA target genes of each term were calculated using the differential miRNA target genes annotated by GO terms. Then, the *p*-value was calculated using the hypergeometric distribution method (the standard for significant enrichment was p-value < 0.05) to find the GO terms of different miRNA target genes with significant enrichment compared to the whole genome background and to determine the main biological functions performed by these miRNA target genes. Results were classified according to molecular functions (MF), biological processes (BP), and cellular components (CC). The first 10 GO term items with the smallest *p*-values (most significant enriched) were selected for each GO classification (Fig. 8).

According to the GO analysis results, the enrichment degree was measured by the rich factor, FDR value, and the number of miRNA target genes enriched on the GO term. The rich factor refers to the ratio. The larger the rich factor, the greater the enrichment degree. The general FDR value range was 0–1. The closer it is to zero, the more significant the enrichment is. The first 20 GO term entries with the lowest FDR values (most significant enriched) were selected for display (Fig. 5A-B).

The enrichment analysis results provided direct acyclic diagrams of the three GO ontologies (cellular components, molecular functions, and biological processes). In this diagram, the closer to the root node, the more general the GO term is. Besides, the GO term branching down is the term annotated at a more precise level. By default, the program sets the top 10 GO terms with the highest significance to be squares, and the other terms to be circles. The darker the color, the more significant the GO term is. The colors from light to dark are: colorless, light yellow, dark yellow, and red (Fig. 5C-H). Additionally, the KEGG pathway enrichment analysis was carried out according to the target gene results. The top 20 pathways with the smallest *p*-value (most significant enriched) were selected for display (Fig. 5I-J).

3.5 RT-qPCR verification

Finally, rno-mir-340-5p, rno-mir-21-5p, rno-mir-145-5p and rno-mir-195-5p expressions were verified by RT-qPCR (Fig. 6). The designed primer sequences are shown in Table 3 and their relative expression levels were analyzed by t-tests with a $p \leq 0.05$ as statistically significant. Compared to pre-operative samples, rno-mir-340-5p and rno-mir-21-5p were significantly upregulated. On the other hand, rno-mir-145-5p and rno-mir-195-5p were significantly downregulated. Then, we predicted their target genes and signaling pathways as described above.

4. Discussion

Compared with other organ transplantations, VCA has a higher acute rejection rate, but most patients can achieve long-term survival through timely treatment [12]. However, VCA mild rejection can damage many

normal tissues, leading to dysfunction and even graft loss. Therefore, early diagnosis and timely treatment are very important for acute rejection. At present, rejection is mainly evaluated by subjective examination and blood indexes. These methods are not enough to directly reflect the current graft state and can not accurately predict the future development trend.

Moreover, miRNAs are non-coding RNAs that can be used as biomarkers of immune responses, *in vivo* index regulation, and tumor development [13, 14]. Also, it has been reported that there is a difference in the expression of plasma miRNAs in acute rejection induced by VCA in rats [15], and the TaqMan miRNA reverse transcription kit has been used to detect the expression of known miRNAs in the skin and other tissues [11]. However, the miRNAs detected by these methods are very limited, and whether other miRNAs are important has not been fully clarified. Therefore, we used miRNA-seq to detect miRNAs that are important during VCA acute immune rejection.

The expression of special miRNA in VCA immune rejection was previously summarized in a review [16]. The roles of rno-mir-142-5p and rno-mir-146a-5p were further confirmed, consistent with the results described in our current research. In addition to these miRNAs, we also found that many new miRNAs are important during acute rejection, such as rno-miR-150-5p, rno-miR-16-5p, rno-miR-21-5p, rno-miR-3068-3p, rno-miR-340-5p, rno-miR-425-5p, rno-miR-451-5p, rno-let-7b-5p, rno-miR-100-5p, rno-miR-125a-5p, rno-miR-125b-2-3p, rno-miR-125b-5p, rno-miR-127-3p, rno-miR-145-3p, rno-miR-145-5p, rno-miR-152-3p, rno-miR-195-5p, rno-miR-196a-5p, rno-miR-196b-5p, and rno-miR-379-5p. We screened four miRNA according to their differential expression and predicted the number of target genes. The RT-qPCR results verified that rno-mir-340-5p and rno-mir-21-5p were upregulated, and rno-mir-145-5p and rno-mir-195-5p were downregulated. Previously, it was reported that rno-mir-340-5p was significantly upregulated in the plasma of a mouse allogeneic transplantation model [17]. Besides, rno-mir-145-5p can help in the diagnose of renal transplantation rejection [18]. The results of our allograft rat models further confirmed their performance in animal models, which might lead to reliable biomarkers for human organ allotransplantation detection.

Also, rno-mir-340-5p and rno-mir-21-5p have many target genes enriched in the PI3K-Akt signaling pathway, which is closely related to corneal transplantation rejection. Additionally, rno-mir-340-5p plays a role in the progression of osteosarcoma through the PI3K Akt pathway [19]. However, the mechanism of rno-mir-340-5p/PI3K-Akt is rarely reported. Whether rno-mir-340-5p and its most abundant target gene regulate VCA acute immune rejection via the PI3K-Akt signaling pathway needs to be further explored. Significantly downregulated rno-mir-145-5p and rno-mir-195-5p were enriched in the Hippo signaling pathway. However, little is known about the role of the Hippo signaling pathway in immune rejection. Loss of Hippo tumor suppressor activity and hyperactivation of Yap are commonly observed in cancers [20]. Tumor and liver-related Hippo's research has been very in-depth. In the future, we can focus on immunity mechanisms.

This study also has some limitations. First, we detected the expression of only four miRNAs. More miRNAs should be detected and the combination of different miRNAs should be analyzed to improve the

specificity and sensitivity of rejection detection. Second, only rat miRNAs were used in this study and, although rats share many genes with humans, they are not the same. Hence, it would be better to have clinical specimens to detect human miRNAs to further assist clinical diagnosis and treatment.

Declarations

Funding

This work was supported by a grant from National Major Science and Technology Projects of China (2018ZX10303502) and National Natural Science Foundation of China (82002065).

Competing Interests

The authors state that the study was conducted without any conflict of interest.

Author Contributions

YF and SW performed the research. YF and SW designed the research study. BS and JC contributed essential reagents or tools. XL, YX and YZ helped to analyze the data. YF wrote the article. SL and JZ revised the article. All authors read and approved the final manuscript.

Data Availability

The datasets generated during or analysed during the current study are available from the corresponding author on reasonable request.

Ethical statement

No human studies were carried out by the authors for this article.

References

1. Charlton, M., et al., *International Liver Transplantation Society Consensus Statement on Immunosuppression in Liver Transplant Recipients.* Transplantation, 2018. **102**(5): p. 727-743.
2. Freitas, N.C.C., et al., *Sixteen Years of Heart Transplant in an Open Cohort in Brazil: Analysis of Graft Survival of Patients using Immunosuppressants.* Arq Bras Cardiol, 2021. **116**(4): p. 744-753.
3. Gander, B., et al., *Composite tissue allotransplantation of the hand and face: a new frontier in transplant and reconstructive surgery.* Transpl Int, 2006. **19**(11): p. 868-80.
4. Huang, C., et al., *MicroRNAs in autoimmune liver diseases: from diagnosis to potential therapeutic targets.* Biomed Pharmacother, 2020. **130**: p. 110558.
5. Goodall, G.J. and V.O. Wickramasinghe, *RNA in cancer.* Nat Rev Cancer, 2021. **21**(1): p. 22-36.
6. Kim, D., et al., *Anti-inflammatory Roles of Glucocorticoids Are Mediated by Foxp3(+) Regulatory T Cells via a miR-342-Dependent Mechanism.* Immunity, 2020. **53**(3): p. 581-596 e5.

7. Hou, G., et al., *SLE non-coding genetic risk variant determines the epigenetic dysfunction of an immune cell specific enhancer that controls disease-critical microRNA expression.* Nat Commun, 2021. **12**(1): p. 135.
8. Neumann, A., et al., *MicroRNA 628-5p as a Novel Biomarker for Cardiac Allograft Vasculopathy.* Transplantation, 2017. **101**(1): p. e26-e33.
9. Ledeganck, K.J., et al., *MicroRNAs in AKI and Kidney Transplantation.* Clin J Am Soc Nephrol, 2019. **14**(3): p. 454-468.
10. Oda, H., et al., *Plasma microRNAs Are Potential Biomarkers of Acute Rejection After Hindlimb Transplantation in Rats.* Transplant Direct, 2016. **2**(11): p. e108.
11. Oda, H., et al., *Relative antigenicity of components in vascularized composite allotransplants: An experimental study of microRNAs expression in rat hind limb transplantation model.* Microsurgery, 2019. **39**(4): p. 340-348.
12. Wang, S., et al., *Evaluation of PLGA microspheres with triple regimen on long-term survival of vascularized composite allograft - an experimental study.* Transpl Int, 2020. **33**(4): p. 450-461.
13. Mikami, Y., et al., *MicroRNA-221 and -222 modulate intestinal inflammatory Th17 cell response as negative feedback regulators downstream of interleukin-23.* Immunity, 2021. **54**(3): p. 514-525 e6.
14. Komoll, R.M., et al., *MicroRNA-342-3p is a potent tumour suppressor in hepatocellular carcinoma.* J Hepatol, 2021. **74**(1): p. 122-134.
15. Oda, H., et al., *MicroRNAs are potential objective and early biomarkers for acute rejection of transplanted limbs in a rat model.* Microsurgery, 2017. **37**(8): p. 930-936.
16. Di Stefano, A.B., et al., *MicroRNAs in solid organ and vascularized composite allotransplantation: Potential biomarkers for diagnosis and therapeutic use.* Transplant Rev (Orlando), 2020. **34**(4): p. 100566.
17. Wu, S.C., et al., *Identification of Circulating miRNAs in a Mouse Model of Nerve Allograft Transplantation under FK506 Immunosuppression by Illumina Small RNA Deep Sequencing.* Dis Markers, 2015. **2015**: p. 863192.
18. Lin, Y., et al., *Multi-omics network characterization reveals novel microRNA biomarkers and mechanisms for diagnosis and subtyping of kidney transplant rejection.* J Transl Med, 2021. **19**(1): p. 346.
19. Tong, C.J., et al., *LncRNA RUSC1-AS1 promotes osteosarcoma progression through regulating the miR-340-5p and PI3K/AKT pathway.* Aging (Albany NY), 2021. **13**(16): p. 20116-20130.
20. Tang, Y., et al., *Selective Inhibition of STRN3-Containing PP2A Phosphatase Restores Hippo Tumor-Suppressor Activity in Gastric Cancer.* Cancer Cell, 2020. **38**(1): p. 115-128 e9.

Figures

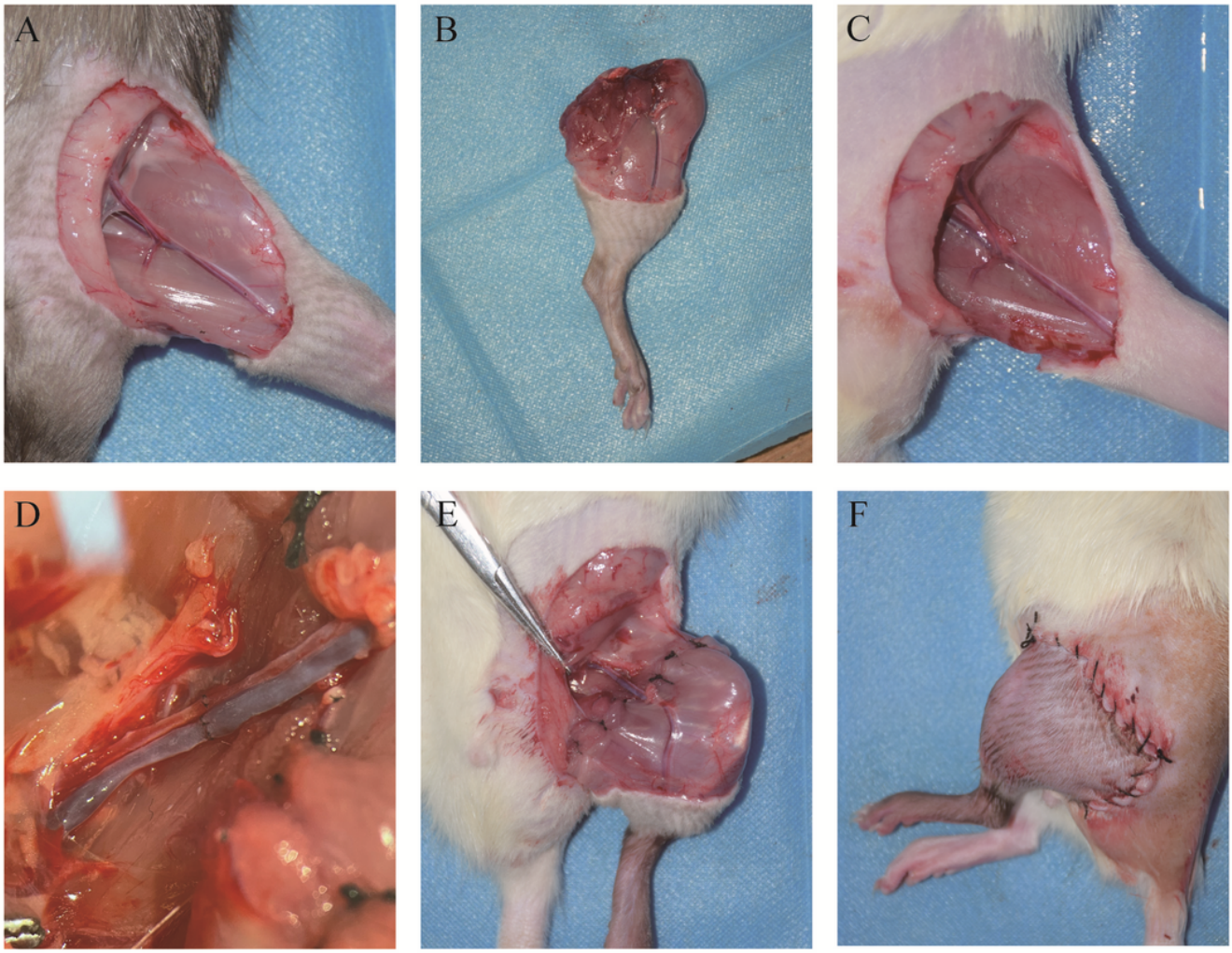

Figure 1

Surgical procedures. (A) Prepare the donor site for amputation. (B) Amputation. (C) Prepare the receptor. (D) Perform vascular anastomosis. (E) and (F) Close muscles and skin.

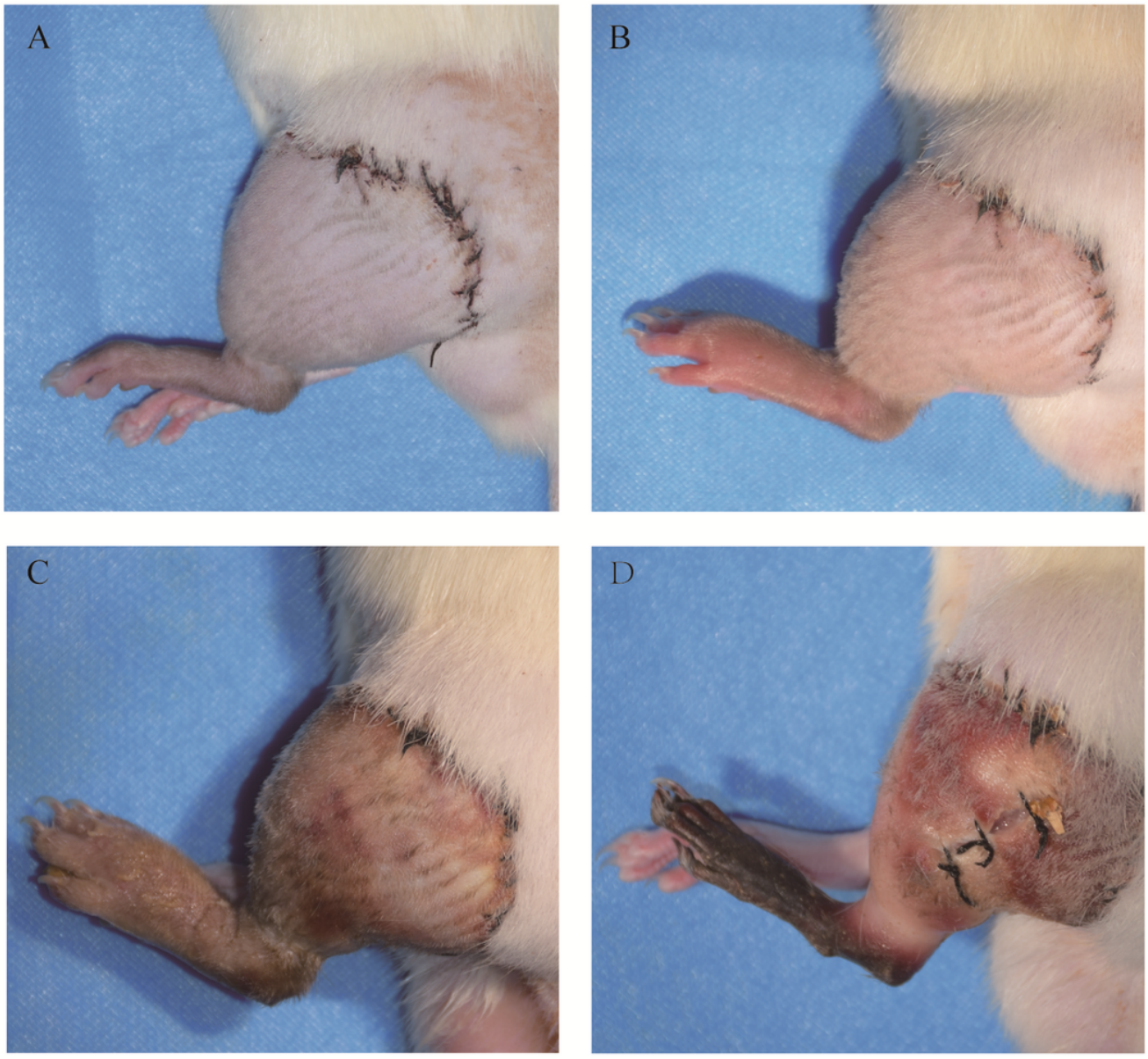

Figure 2

Allograft images at post-operative days 3 (A), day 7 (B), day 10 (C) and day 14 (D).

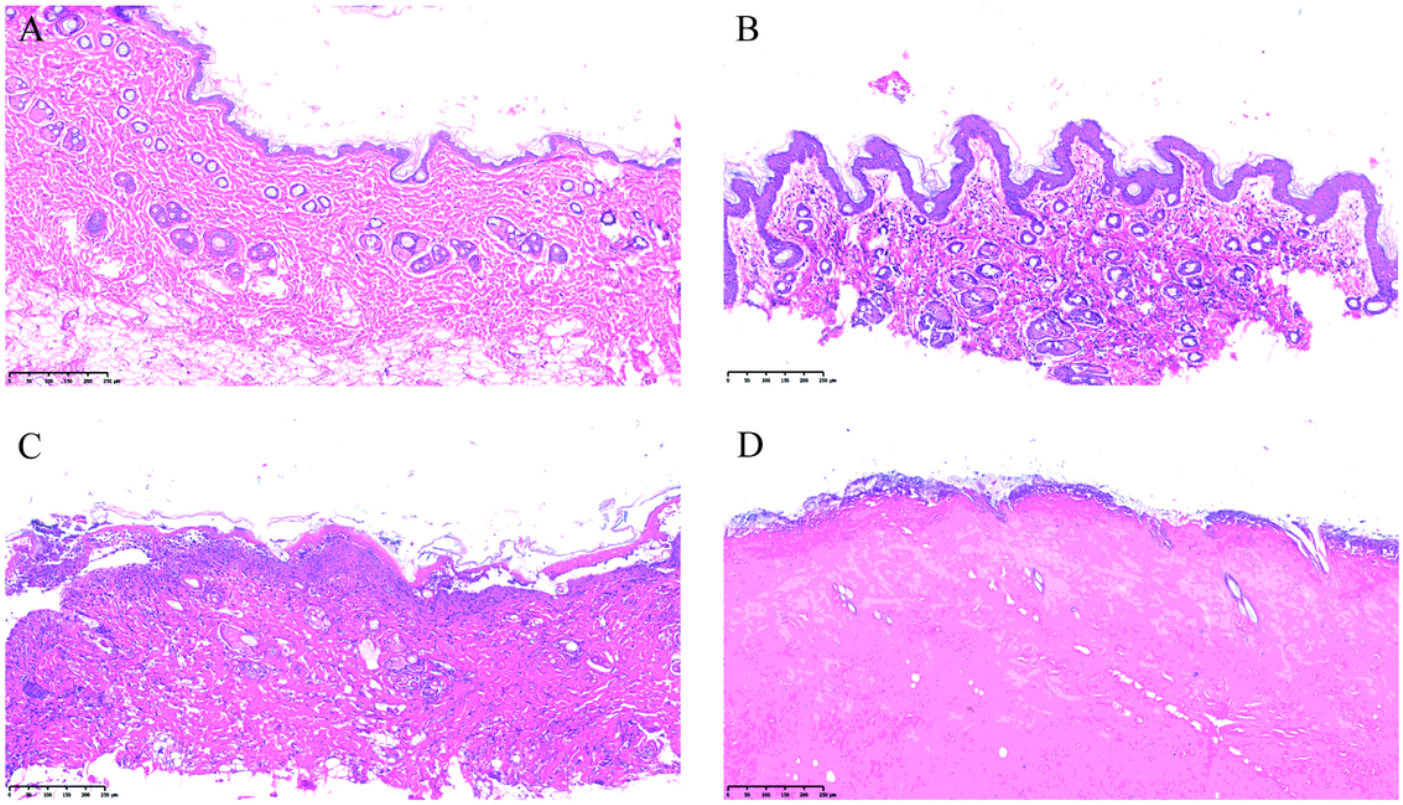

Figure 3

Hematoxylin and eosin staining of skin samples. Allograft skin tissues at days 0 (A), day 7 (B), day 10 (C) and day 14 (D). Bar; 250 μm.

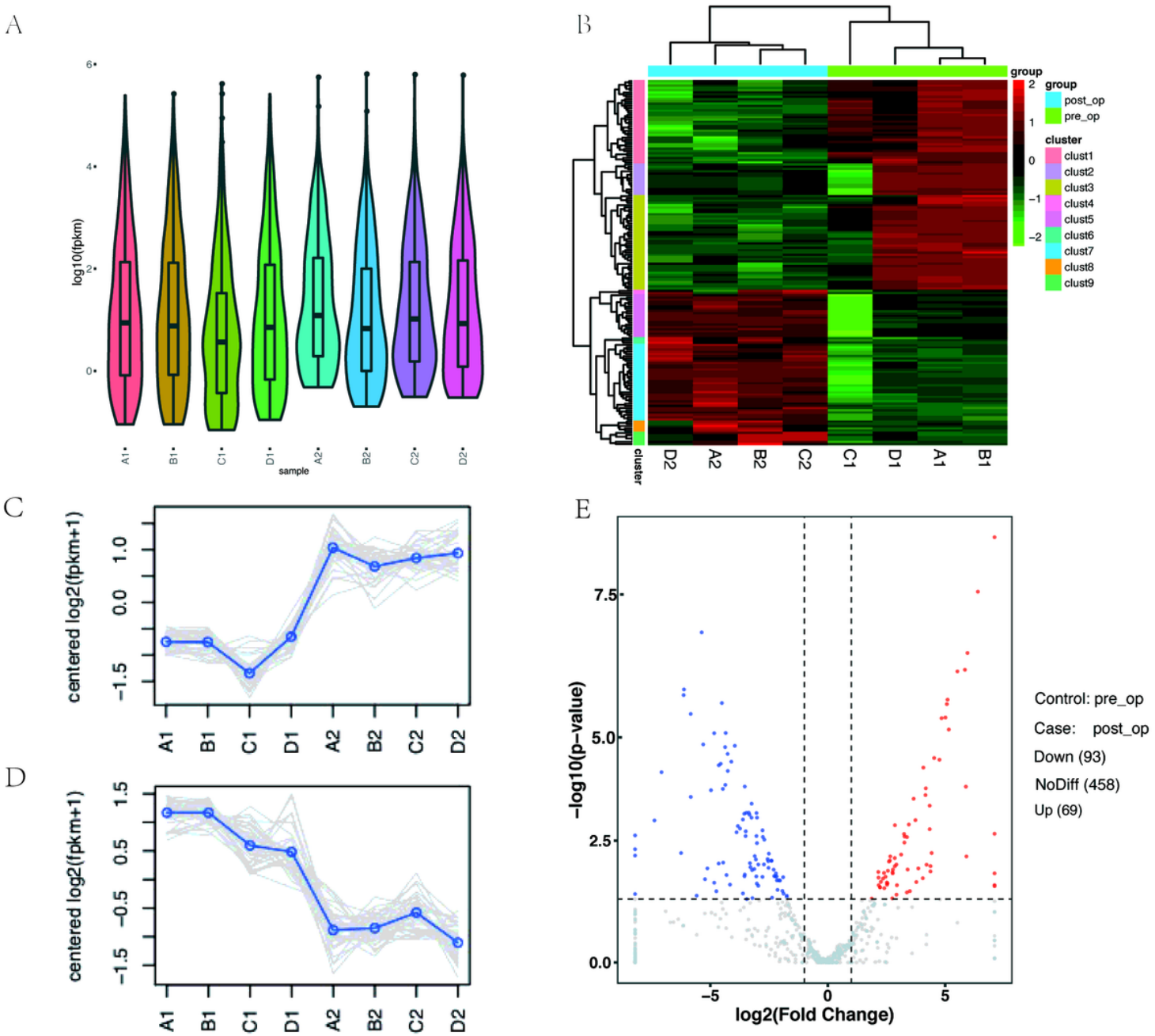

Figure 4

(A) The horizontal line in the middle of the box is the median. The upper and lower edges of the box are 25% and 75% respectively, and the upper and lower limits are 10% and 90% respectively. The external shape is kernel density estimation. (B) Differential expression miRNA clustering. Horizontal represents miRNA, and each column is a sample. Red represents high expression miRNA and green represents low expression miRNA. (C-D) Trend analysis. The gray line in the figure shows the expression pattern of genes in each cluster, and the blue line represents the average expression of all genes in the cluster in the sample. (E) Volcano diagram of differentially expressed genes. The abscissa is -log10 (p-value) and the

ordinate is -log10 (p-value). The two vertical dashed lines in the figure are twice the expression difference threshold; The horizontal dotted line is p-value=0.05 threshold. The red dot indicates the up-regulated genes, the blue dot indicates the down-regulated genes, and the gray dot indicates the nonsignificant differentially expressed genes.

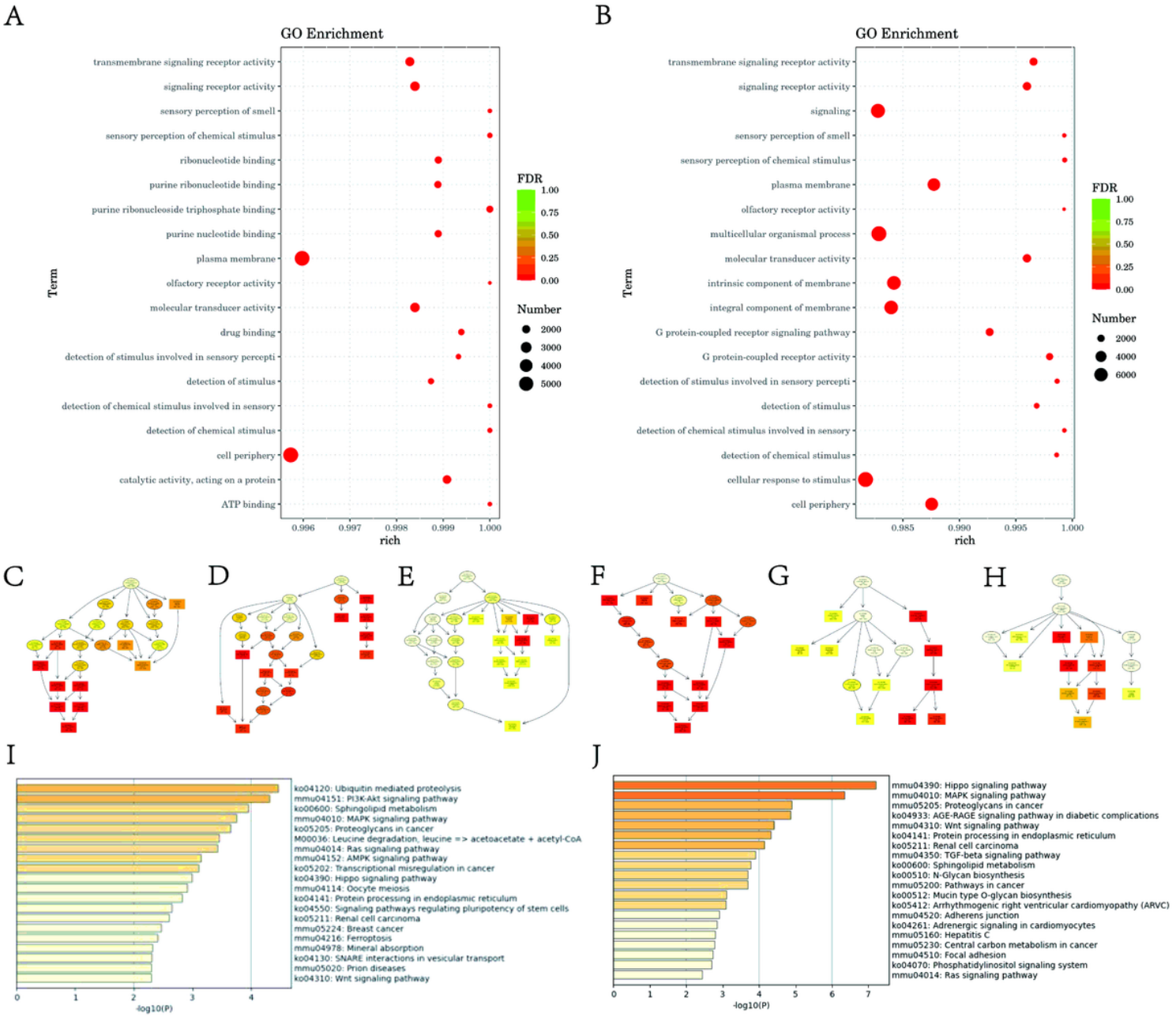

Figure 5

Bubble Diagram of GO enrichment analysis in up-regulated (A) and down-regulated (B) miRNA. (C-H) Up-regulated gene ontology DAG enrichment map of biological process (C), molecular function (D) and cell component (E). Down-regulated gene ontology DAG enrichment map of biological process (F), molecular function (G) and cell component (H). Each node represents a GO term, and branches represent inclusion

relations. The function range defined from top to bottom is becoming smaller and smaller. The box represents the GO term with the enrichment degree of TOP10, and the darker the color, the higher the enrichment degree. (I-J) Histogram of KEGG pathway enrichment results in up-regulated (I) and down-regulated (J) miRNA. The abscissa is the name, and the ordinate is - log10 (p-value) of each pathway.

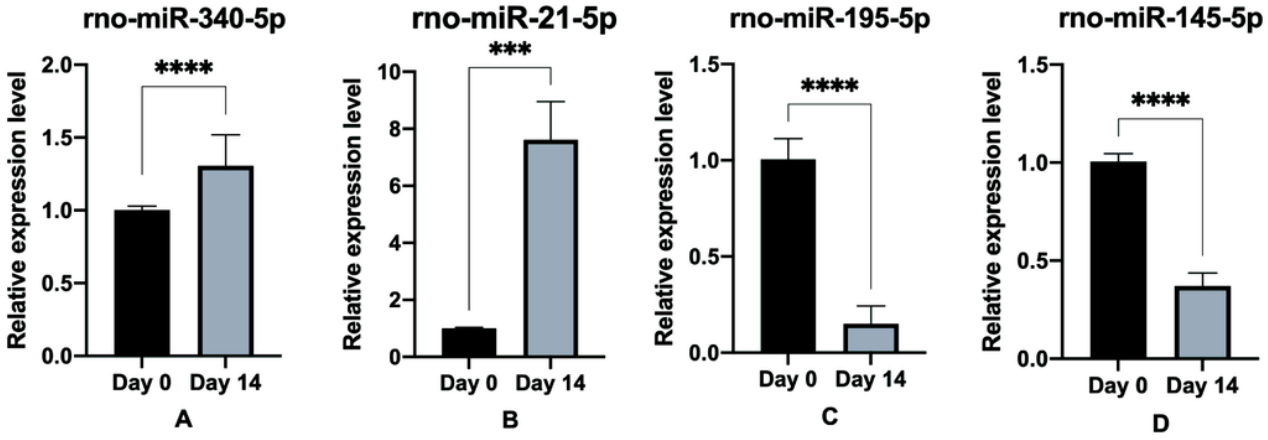

Figure 6

Validation of the four selected miRNAs using RT-qPCR verification. Compared with the day 0th, (A-B) rno-miR-340-5p and rno-miR-21-5p were up-regulated; (C-D) rno-miR-145-5p and rno-miR-195-5p were down-regulated. The data were normalized using the mean ± standard error of the mean (SEM). ***P ≤0.001, **** P ≤0.0001.